

MECHANISM OF THE HYDROXYL RADICAL OXIDATION OF
METHACRYLOYL PEROXYNITRATE (MPAN) AND ITS
PATHWAY TOWARD SECONDARY ORGANIC AEROSOL
FORMATION IN THE ATMOSPHERE

Nguyen, T. B., K. H. Bates, J. D. Crouse, R. H. Schwantes, X. Zhang, H. G. Kjaergaard, J. D. Surratt, P. Lin, A. Laskin, J. H. Seinfeld, and P. O. Wennberg (2015). "Mechanism of the hydroxyl radical oxidation of methacryloyl peroxy-nitrate (MPAN) and its pathway toward secondary organic aerosol formation in the atmosphere". In: *Phys. Chem. Chem. Phys.* 17.27, pp. 17914–17926. doi: 10.1039/C5CP02001H.

Abstract

Methacryloyl peroxy-nitrate (MPAN), the acyl peroxy-nitrate of methacrolein, has been suggested to be an important secondary organic aerosol (SOA) precursor from isoprene oxidation, but the mechanism by which MPAN produces SOA through reaction with the hydroxyl radical (OH) remains unclear. We systematically evaluate three proposed mechanisms in controlled chamber experiments and provide the first experimental support for the theoretically-predicted lactone formation pathway from the MPAN + OH reaction, producing hydroxymethyl-methyl- α -lactone (HMML). The decomposition of the MPAN-OH adduct yields HMML + NO₃ (~75%) and hydroxyacetone + CO + NO₃ (~25%), out-competing its reaction with atmospheric oxygen. The production of other proposed SOA precursors, *e.g.* methacrylic acid epoxide (MAE), from MPAN and methacrolein are negligible (<2%). Furthermore, we show that the β -alkenyl moiety of MPAN is critical for lactone formation. Alkyl radicals formed cold *via* H-abstraction by OH do not decompose to HMML, even if they are structurally identical to the MPAN-OH adduct. The SOA formation from HMML, from polyaddition of the lactone to organic compounds at the particle interface or in the condensed phase, is close to unity under dry conditions. However, the SOA yield is sensitive to particle liquid water and solvated ions. In hydrated inorganic particles, HMML reacts primarily with H₂O to produce the monomeric 2-methylglyceric acid (2MGA) or with aqueous sulfate and nitrate to produce the associated organosulfate and organonitrate, respectively. 2MGA, a tracer for isoprene SOA, is semivolatile and its accommodation in aerosol water decreases with

decreasing pH. Conditions that enhance the production of neutral 2MGA suppress SOA mass from the HMML channel. Considering the liquid water content and pH ranges of ambient particles, 2MGA will exist largely as a gaseous compound in some parts of the atmosphere.

C.1 Introduction

Anthropogenic emissions of nitrogen oxides ($\text{NO}_x = \text{NO} + \text{NO}_2$) strongly influence the oxidative pathways of gaseous hydrocarbons from both natural and anthropogenic origins. In particular, the oxidation of isoprene (C_5H_8), arguably the most important non-methane hydrocarbon emitted to the atmosphere, has a significant sensitivity to the NO_x conditions under which it is oxidized. This NO_x sensitivity translates to regional environmental impacts. For example, the high- NO_x oxidation of isoprene controls the production of tropospheric ozone in regions rich with biogenic hydrocarbons (Browne and Cohen, 2012; Mao *et al.*, 2013; Pusede and Cohen, 2012) by accelerating the cycling of NO_x and producing NO_x reservoir species (*e.g.* organic nitrates and peroxy nitrates). Isoprene chemistry also affects global climate primarily through the formation of secondary organic aerosol (SOA) (Carlton and Turpin, 2013; Goldstein *et al.*, 2009; Rollins *et al.*, 2012; Xu *et al.*, 2015). However, lingering uncertainties regarding SOA formation in various anthropogenically impacted but biogenically influenced systems preclude accurate simulations of human-induced climate and air quality feedbacks in atmospheric chemical transport models.

A common approach to identify the source of SOA is through tracer compounds, *e.g.* 2-methylglyceric acid (2MGA) in isoprene-derived ambient aerosols (Edney *et al.*, 2005; Ion *et al.*, 2005; Kourtchev *et al.*, 2005). 2MGA and its oligomers are thought to be enhanced under high- NO_x conditions, and can be uniquely traced to the oxidation of methacrolein, a first-generation isoprene oxidation product (Chan *et al.*, 2010a; Claeys *et al.*, 2004; Nguyen *et al.*, 2011b; Surratt *et al.*, 2006). Chan *et al.* (2010a) showed that high- NO_2 chemistry (as opposed to "high- NO_x ", where most of the NO_x can be represented by NO) favours the production of SOA *via* the acyl peroxy nitrate channel (APN, Figure C.1). Essentially all of the SOA generated in the laboratory studies of the isoprene high- NO_x route was shown to be derived from methacrolein photochemistry, suggesting a major role of the APN from methacrolein, methacryloyl peroxy nitrate (MPAN). The suggestion by Chan *et al.* (2010a) was confirmed by the synthesis of MPAN and the measurement of its SOA formation through photochemistry (tested under high-NO conditions) (Surratt

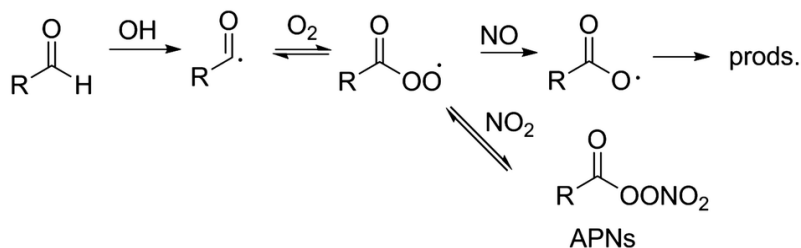


Figure C.1: The formation of acyl peroxy nitrates (APNs) from the OH-initiated oxidation of aldehydes is favored under high NO_2/NO conditions. For methacrolein, the abstraction of the aldehydic H occurs roughly half of the time in the OH oxidation reaction at room temperature (Orlando *et al.*, 1999).

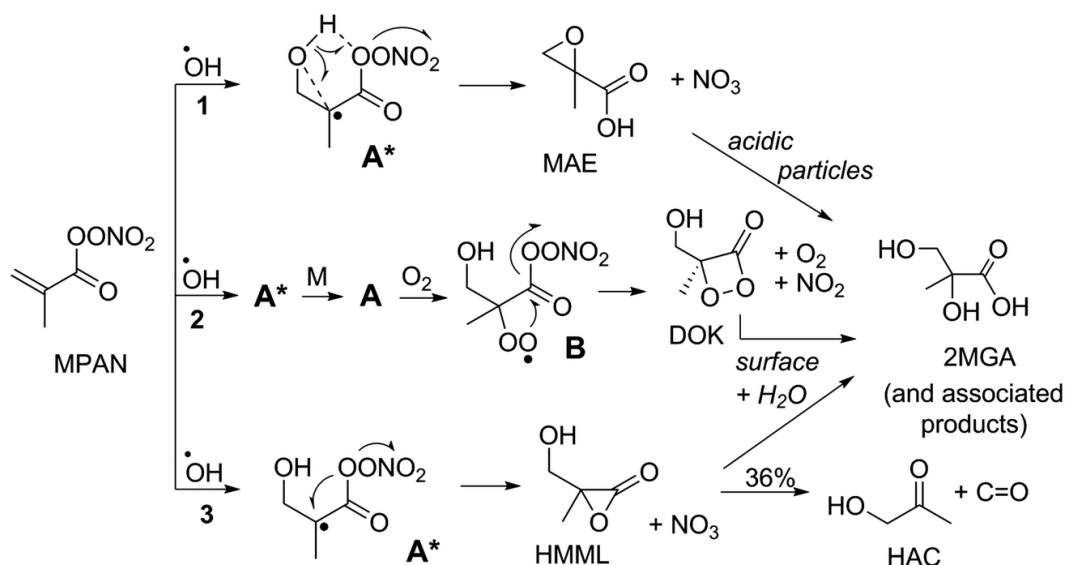


Figure C.2: The three proposed pathways to the formation of 2-methylglyceric acid (2MGA), a tracer for isoprene-derived ambient SOA. Mechanisms 1-3 and acronyms are discussed in the text.

et al., 2010).

Although the potential of MPAN + OH chemistry to produce SOA is relatively well established, the chemical mechanism leading to SOA from MPAN photooxidation has been subject of debate. It is also not clear whether the MPAN photooxidation is sensitive to NO_x , although past studies have all been performed in the presence of NO. Figure C.2 shows three possible pathways leading to SOA production that have been proposed by independent works (Chan *et al.*, 2010a; Kjaergaard *et al.*, 2012; Lin *et al.*, 2013b).

The initial step of the MPAN photooxidation is OH addition to the double bond,

primarily generating the energetically hot tertiary alkyl radical of MPAN (A^* , Figure C.2). Chan *et al.* (2010a) in a series of photochemical chamber experiments, proposed that the main fate of A^* is collisional stabilization (producing A) followed by reaction with molecular oxygen to form an alkylperoxyl radical (B), where the β -peroxyl moiety attacks at the carbonyl carbon to form a dioxoketone (DOK) and NO_2 as a coproduct (Figure C.2, mechanism 2). The suggestion by Chan *et al.* (2010a) was derived by performing methacrolein high- NO_2 photooxidation experiments at low O_2 content ($\sim 2\%$). The authors did not observe an increase in SOA yield and concluded that either O_2 addition is required for SOA formation or is non-competitive at those levels.

From a combined suite of density functional theory and coupled cluster calculations, Kjaergaard *et al.* (2012) proposed a rapid ring closure from an acylperoxyl oxygen of A^* to form a 3-member lactone, hydroxymethyl-methyl- α -lactone (HMML), and NO_3 as a coproduct (Figure C.2, mechanism 3). Furthermore, the authors hypothesize that a significant fraction of the HMML product (36%) is generated with sufficient energy to further decompose to hydroxyacetone (HAC) and CO. Lin *et al.* (2013b) also identified the formation of HMML *via* density functional theory calculations; however, they hypothesized that HMML may be too unstable to form in the atmosphere.

Lin *et al.* (2013b) proposed a rapid H-migration induced ring closure at the hydroxyl oxygen, *via* a 6-member intermediate, to an epoxide product called methacrylic acid epoxide (MAE, Figure C.2, mechanism 1). This suggestion was formulated by comparing the composition of SOA (*e.g.* 2MGA and other products) from the photooxidation of methacrolein and the reactive uptake of laboratory-synthesized MAE onto highly-acidic particles, as well as through quantum chemistry calculations. The mechanism of the uptake was suggested to be nucleophilic ring opening of the epoxide in an analogous reaction to the isoprene epoxydiols (Paulot *et al.*, 2009b).

Notable differences between the proposed pathways include: (1) the fate of A^* – whether cyclization/decomposition occurs more rapidly than thermalization and, thus, bimolecular reaction with O_2 , (2) the stability of the products – MAE is the only product stable enough to be detected by current analytical instrumentation, and (3) the subsequent SOA formation mechanism under low humidity conditions – MAE requires highly-acidic seed aerosols to open the epoxide ring, while the ring opening of the more unstable compounds, DOK and HMML, would likely require

only collisions with a surface.

The uncertainties in the MPAN + OH mechanism persist due to ambiguities from previous work. For example, earlier studies of the MPAN + OH system did not measure SOA formation and were conducted with high mixing ratios of NO_x (blind to the formation of nitrogen products) (Grosjean *et al.*, 1993c; Orlando *et al.*, 2002). More recent laboratory studies of Chan *et al.* (2010a) and Lin *et al.* (2013b) were performed with methacrolein, such that products from MPAN oxidation and from the OH addition route of methacrolein (~55% probability) were formed simultaneously, complicating the analysis (Orlando *et al.*, 1999). The theoretical study of Kjaergaard *et al.* (2012) has yet to be experimentally validated. In this work, we elucidate the chemical mechanism governing the MPAN photooxidation (and the photooxidation of its chemical analogues) through a series of targeted chamber experiments using laboratory-synthesized MPAN under low humidity and low-NO conditions. We further study the chemical pathway with which the MPAN produces SOA under simulated ambient conditions with higher relative humidity and seed particle concentrations.

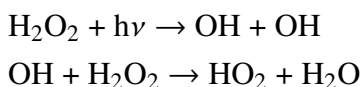
C.2 Experimental

C.2.1 Chamber Studies

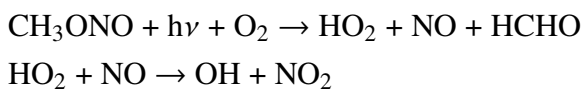
The atmospheric chamber facility used for this work has been described in detail (Nguyen *et al.*, 2014b). A portion of the present work, namely, control experiments with α -pinene and exploratory experiments with methacrolein, were performed as part of the Focused isoprene eXperiment at the California Institute of Technology (FIXCIT) chamber campaign (Nguyen *et al.*, 2014b). Briefly, experiments were conducted in a large (24 m³) Teflon chamber using purified dry air (<5% relative humidity (RH) at 298 K) such that initial NO mixing ratios were lower than 100 pptv (measured by G. S. Tyndall, D. D. Montzka, and A. J. Weinheimer at FIXCIT) and initial particle mass concentrations were much lower than 0.01 $\mu\text{g m}^{-3}$ (measured by SMPS). For the experiments that were performed under humid conditions, water vapor was added to the chamber using a Nafion membrane humidifier (Perma Pure LLC) and recirculating ultrapure water (18 M Ω , Millipore Milli-Q). Particles were injected (mean particle diameter ~70 nm) by atomizing dilute solutions of ammonium sulfate (0.1 M) through a heated wet-wall denuder to deliquesce the particles prior to entering the chamber held at RH 40% or 85%. Corrections for the wall deposition of particles, using ammonium sulfate seed aerosols, were derived from control experiments performed at several water vapor mixing ratios in the

chamber. Volatile organics, excluding MPAN, were injected by microliter syringe into a clean glass bulb and quantitatively transferred with dry nitrogen gas into the chamber through a short section of tubing, optionally with gentle heating for the larger hydrocarbons such as α -pinene (<80 °C). The temperature in the chamber enclosure was adjusted to 15-25 °C for experiments as needed. MPAN experiments were performed at 15 °C to minimize the thermal decomposition of MPAN (thermal lifetime ~ 26 h at 15 °C, compared to ~ 5 h at 25 °C, for an NO_2/NO ratio of 10 that is representative of areas outside of urban centers) (Roberts and Bertman, 1992).

Table C.1 lists the laboratory conditions for the main experiments in this work, *e.g.* the gas-phase oxidation of MPAN (synthesized standard), methacrolein (MACR, Aldrich, 95%), isobutyraldehyde (ISOBUT, Aldrich, $>99\%$), and 2-methylbut-3-ene-1-ol (231MBO, Aldrich, 98%). Photochemistry under low-NO conditions ($\text{HO}_2 > \text{NO}$) was initiated by the near-UV (300-400 nm, $\lambda_{max} \sim 350$ nm) photolysis of gas-phase hydrogen peroxide that has been evaporated into the chamber (Aldrich, 50 wt% in water):



Photochemistry under high NO_2 (and typically lower in NO) conditions were initiated by the photolysis of gas-phase methyl nitrite (synthesized standard, stored in liquid N_2) in the presence of various mixing ratios of additional NO_2 (standard mixture in N_2):



Methyl nitrite was introduced into the chamber by filling a clean, evacuated, 500 mL glass bulb with the desired pressure of the standard, backfilling with N_2 , and transferring the contents of the bulb into the chamber with a stream of N_2 . In high- NO_2 experiments, the added NO_2 and that formed from CH_3ONO photochemistry conspire to maintain the NO_2/NO ratio >10 throughout the experiment. Importantly, the near-UV broadband radiation used in this work does not efficiently photolyze NO_3 *via* mechanisms that yield a net destruction of NO_3 ($J_{\text{NO}_2} \sim 5.5 \times 10^{-4} \text{ s}^{-1}$, $J_{\text{NO}_3 \rightarrow \text{NO} + \text{O}_2} \sim 4.5 \times 10^{-6} \text{ s}^{-1}$) (Sander *et al.*, 2011).

C.2.2 Analytical Measurements

MACR and isobutyraldehyde were quantified with a commercial gas chromatograph with a flame-ionization detector (GC-FID, HP 6890N) and calibrated by

expt. #	HC precursor		oxidant		[OH] _{ss} (cm ⁻³)	rxn time (h)	temp. (°C)	RH (%)	[NO] ₀ (ppb)	[NO ₂] ₀ (ppb)	additional injections
	name	[HC] ₀ (ppb)	source	[Ox] ₀ (ppb)							
1	MPAN	30	H ₂ O ₂ + hν	2000	1.5 × 10 ⁶	2.5	15	<5	<0.1	1	α-Pin (50 ppb)
2	MPAN	13	H ₂ O ₂ + hν	2000	1.5 × 10 ⁶	5	15	<5	<0.1	1	-
3	MPAN	23	H ₂ O ₂ + hν	2000	1.5 × 10 ⁶	4.5	15	<5	<0.1	1	-
4	MPAN	30	H ₂ O ₂ + hν	2000	1.5 × 10 ⁶	4.5	15	<5	<0.1	1	α-Pin (30 ppb), MAE (15 ppb)
5	MPAN	17	H ₂ O ₂ + hν	2000	1.5 × 10 ⁶	3.2	15	<5	<0.1	1	α-Pin (30 ppb), MAE (15 ppb)
6	MACR	100	H ₂ O ₂ + hν	2000	1.5 × 10 ⁶	5	15	<5	10	230	-
7	MACR	50	MN + hν	140	2 × 10 ⁷	2.5	25	<5	<0.1	50	-
8	MACR	80	MN + hν	130	1 × 10 ⁷	2.5	15	<5	<0.1	110	-
9	MACR	100	MN + hν	200	2 × 10 ⁷	2.5	25	<5	10	100	-
10	ISOBUT	80	MN + hν	220	2 × 10 ⁷	5.5	25	<5	10	50	-
11	231MBO	200	O ₃ , then MN + hν	~600 [O ₃], 200 [MN]	2 × 10 ⁷	24	25	<5	10	100	-
12	MACR	200	MN + hν	200	2 × 10 ⁷	3.5	25	40	10	100	AS seeds
13	MACR	100	MN + hν	200	2 × 10 ⁷	2.5	25	85	10	100	AS seeds

Table C.1: Experimental conditions for the laboratory photooxidation of hydrocarbons (HC) used in this work: MPAN, methacrolein (MACR), isobutyraldehyde (ISOBUT) and 2-methylbut-3-ene-1-ol (231MBO). The light intensity was 100% ($J_{NO_2} \sim 7 \times 10^{-3} \text{ s}^{-1}$) for hydrogen peroxide (HP) experiments and 10-20% for methyl nitrite (MN) experiments. Steady state OH is estimated from hydrocarbon decay (GC) data. α -pinene (α -Pin) and methacrylic acid epoxide (MAE) were added in select experiments to capture NO₃ and observe SOA formation, respectively. Control experiments of HP + hν, tridecane + HP + hν, and wall losses (described in Experimental section) are not included in table. Experiments were performed at various temperature and relative humidity (RH). Select experiments were performed with $\sim 80 \mu\text{g m}^{-3}$ of ammonium sulfate (AS) seed particles.

volumetric injections of commercial standards. Particle size and number were measured by a scanning mobility particle sizer (SMPS), *i.e.* a custom-built differential mobility analyzer coupled to a commercial condensation particle counter (TSI Inc.). Aerosol speciation was measured using a high resolution time-of-flight aerosol mass spectrometer (AMS, Aerodyne) (Drewnick *et al.*, 2005). Bulk aerosol species (organic, sulfate, ammonium, nitrate) were calculated using AMS data analysis modules (Pika 1.14D). The instrument's ionization efficiency was calibrated with 350 nm ammonium nitrate particles.

Volatile acids and select polar organic compounds were quantified with a custom-built triple-quadrupole chemical ionization mass spectrometer (CIMS, Agilent/Caltech) (St. Clair *et al.*, 2010). The CIMS operated in three modes: scanning negative ion mode using CF_3O^- as the reagent (m/z 50-250), scanning positive ion mode using primarily H_3O^+ as the reagent ion (m/z 50-200), and tandem mass negative ion mode (monitoring select precursor-product ion pairs). The ion chemistry (*e.g.* detection as $[\text{M}+\text{F}]^-$ and $[\text{M}+\text{CF}_3\text{O}]^-$ ions) and tandem mass determinations of the CF_3O^- CIMS have been described previously (Crouse *et al.*, 2006; St. Clair *et al.*, 2010).

Sensitivities of the triple-quadrupole CF_3O^- CIMS used in this work were determined based on a calibrated time-of-flight CF_3O^- CIMS instrument during the FIX-CIT campaign (Nguyen *et al.*, 2014b). The absolute calibration for commercially-available and synthesized standards in the time-of-flight CIMS, using gravimetric, optical, and thermal-dissociation + laser-induced fluorescence methods are described elsewhere (Nguyen *et al.*, 2015a). Uncertainty is estimated to be $\pm 30\%$. Synthesized standards of organic nitrates were found to have water-dependent sensitivities similar to HNO_3 (Lee *et al.*, 2014); thus the CIMS sensitivity of the pinene nitrooxyhydroperoxide (PNP), for which there are no authentic standards, is assumed to be similar to HNO_3 (estimated uncertainty $\pm 50\%$). For other compounds discussed in this work, theoretical calculations were used to estimate the sensitivity (estimated uncertainty $\pm 50\%$) (Garden *et al.*, 2009; Su and Chesnavich, 1982).

The observed ion of methacrylic acid epoxide (MAE, synthesized standard, detected as $[\text{MAE}\cdot\text{F}]^-$) was isobaric with a water cluster $[(\text{H}_2\text{O})_2\cdot\text{CF}_3\text{O}]^-$ (m/z 121) in the single-ion analysis (Lin *et al.*, 2013b). Thus, MAE quantification is performed with collision-induced dissociation into its main precursor \rightarrow product ion (m/z 121 \rightarrow m/z 101). When experiments are performed at higher relative humidity, the water signal (m/z 121 \rightarrow m/z 103) may have an extensive tail that would lead to an over-

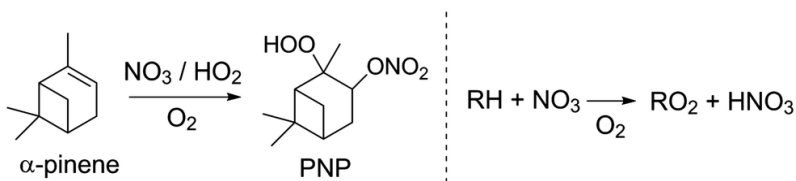


Figure C.3: The experimental scavenging of NO_3 into stable products detectable by CIMS: PNP (one of several isomers shown) and HNO_3 .

estimation of MAE. The tandem signal that we measure must then be considered as an upper limit to the MAE concentration. The ion chemistry in the positive ion mode is similar to proton transfer reaction mass spectrometry (quantification mainly with $[\text{M}+\text{H}]^+$ ions in this work) (Lindinger and Jordan, 1998). Calibrations for select species in the positive ion mode (*e.g.* α -pinene and 231MBO) were performed immediately prior to experiments using commercial standards under dry conditions.

CIMS was also used to indirectly monitor nitrogen oxide chemistry (Figure C.3). For example, the reaction of NO_2 with HO_2 generates peroxyacetic acid (HO_2NO_2 , PNA), which was used as a sensitive tracer for NO_2 . α -pinene was used in a subset of experiments to capture NO_3 as the pinene nitrooxy hydroperoxide (PNP), which is detectable by CIMS, under the condition where the HO_2/NO ratio is high (Figure C.3, left). α -pinene was chosen as an NO_3 scavenger because its reaction rate coefficient with OH is the lowest for a monoterpene that reacts rapidly with NO_3 (*i.e.* $k_{\text{NO}_3}/k_{\text{OH}} \sim 0.12$) (Atkinson *et al.*, 2006), and its reaction rate with NO_3 is at least four orders of magnitude larger than the MPAN reaction with NO_3 (Canosa-Mas *et al.*, 1999b). There are varying reports of SOA yield from the α -pinene + NO_3 reaction (0-16%), possibly decreasing with higher RH (Fry *et al.*, 2014; Hallquist *et al.*, 1999; Spittler *et al.*, 2006). Thus, experiments involving α -pinene were not included in the yield calculations from MPAN due to the possibility of interference from the α -pinene + OH or + NO_3 reaction. HNO_3 , produced from H-abstraction chemistry of hydrocarbons (Figure C.3, right) when NO_2 is low (and thus $\text{NO}_2 + \text{OH}$ is not a significant source of HNO_3), was also used as tracer for NO_3 -initiated chemistry.

MPAN, peroxyacetyl nitrate (PAN), and NO_2 were measured with a commercial NO_2 and acyl peroxyacetyl nitrate (NO_2/APN) analyzer (Fitz Aerometric Technologies). In the NO_2/APN instrument, NO_2 , PAN, and MPAN were chromatographically separated, in that order, with a room-temperature deactivated DB-5 column, and detected by monitoring chemiluminescence from their reactions with luminol (Figure

C.11 in the Supporting Information). NO_2 was calibrated with a diluted standard mixture (488 ppmv NO_2 in N_2 , Scott Specialty Gases). The sensitivity of PAN in the instrument was inferred from its relationship to NO_2 (Gaffney *et al.*, 1998). MPAN, in isolation, was calibrated using a commercial NO_x analyzer (Teledyne model T200) due to its quantitative decomposition to NO_2 when exposed to the heated (310 °C) molybdenum catalyst. A similar calibration was obtained by thermally decomposing MPAN to NO_2 in a heated stainless steel tube before the NO_2 /APN analyzer. Sampling MPAN from the chamber (before adding other compounds) through room-temperature Teflon tubing leads to a small decomposition yield of NO_2 from MPAN (~4%, Figure C.11 in the Supporting Information). The NO_2 signal was corrected in the NO_2 /APN data as a fraction of the MPAN integrated peak.

C.2.3 MPAN

The synthesis of MPAN from the peroxidation of methacrylic anhydride (Aldrich, 94%) and nitration of the methacrylic peracid (MPAA) was performed as suggested by Bertman and Roberts (1991) with the following revisions: we used 50 wt% H_2O_2 (Aldrich) instead of 30 wt% H_2O_2 and methanesulfonic acid (Aldrich, 99.5%) instead of concentrated H_2SO_4 . The crude MPAN mixture in water-tridecane was stored frozen and separated in small fractions with tridecane on a silica gel column deactivated by successive solvent washes of methanol, acetone, ethyl acetate, hexanes, and tridecane. Signs of known impurities were checked by CIMS (*i.e.* methacrylic acid and MPAA) and the NO_2 /APN instrument (PAN). MPAN is thought to be explosive when pure (Stephens, 1969) and no attempt was made to remove the solvent. The separated MPAN fraction in tridecane was stored at 0 °C or below and used promptly.

MPAN was injected by gently bubbling air through the tridecane-solvated mixture (submerged in an ice bath) placed inside the 15 °C chamber enclosure over the course of roughly 30 min to achieve 15-30 ppbv in the chamber. Tridecane was chosen as the storage solvent due to its low volatility, and thus, lower extent of co-evaporation into the chamber. To correct for any SOA originating from photooxidation of the solvent, we performed a control photooxidation experiment with tridecane + OH similarly to Expt. 2-3. The CIMS signals of tridecane (positive mode) and tridecane hydroperoxide (negative mode) were used to normalize the 10-50% correction of tridecane-derived SOA in MPAN experiments.

C.2.4 2MGA

2-Methylglyceric acid (2MGA) was synthesized and purified according to An *et al.* (1992) *via* oxidation of the C=C bond of methacrylic acid (Aldrich, 99%) using H_2WO_4 (Aldrich, 99%) and 50 wt% H_2O_2 (Aldrich). Proton NMR (in DMSO-d_6) was used to verify the isolated 2MGA with residual CH_3CN (93% 2MGA, Figure C.12a in the Supporting Information). The semi-pure 2MGA (viscous liquid) was then crystallized upon cooling, filtered with CH_3CN , and washed with Et_2O to afford the pure (99%) 2MGA crystalline solid. The CIMS observes 2MGA at the fluoride transfer ion ($\text{C}_4\text{H}_7\text{O}_4\cdot\text{HF}^-$) and collision-induced dissociation leads primarily to the deprotonated 2MGA ion ($\text{C}_4\text{H}_7\text{O}_4^-$, Figure C.12b in the Supporting Information). The gas-phase signal of a 2MGA aqueous solution was measured at various solution pH values in a custom 10 mL glass vial fitted with 3 mm O.D. PTFE sampling tubes. A 0.075 M solution of 2MGA had similar pH to glyceric acid (pKa 3.5 (Serjeant and Dempsey, 1979)) at the same concentration. The 2MGA solution was further acidified incrementally by adding droplets of 1-10 wt% H_2SO_4 and the pH of the solution was measured with a digital pH meter (VWR, Model 8015) that had been calibrated with commercial buffer solutions. The headspace of the vial (at 24 °C) was sampled with CIMS at a flow rate of 147 std $\text{cm}^3 \text{ s}^{-1}$ for each solution pH.

C.2.5 High-Resolution Mass Spectrometry

At the end of photooxidation experiments, SOA samples were collected on hydrophilic PTFE-based membrane filters (Millipore, Omnipore, 0.2 μm diameter pores) by pulling chamber air through an activated charcoal denuder, vacuum-sealed, and frozen for further analysis. The SOA material on the filters was gently extracted by wetting with 100-300 μL of acetonitrile and water mixture (2:5 v/v, HPLC grades) for roughly 5 min. The filters were not exposed to heat or ultra-sonication conditions (which may produce free radicals such as OH through cavitation (Makino *et al.*, 1982)) in order to preserve organic species. The extracts were analyzed with high-performance liquid chromatography (HPLC) coupled to electrospray ionization mass spectrometry (ESI-MS). The separation was performed with a polar embedded C_{18} column with TMS endcapping (Phenomenex, SynergiTM 4 μm Fusion-RP 80 Å, 150 \times 2.0 mm) and an eluent mixture of acetonitrile and water (HPLC grades, Aldrich) with 0.5% of formic acid. Generally, the organic constituents eluted together (*e.g.* the entire oligomer family of 2-methylglyceric acid in the MPAN + OH samples) but are satisfactorily separated from the inorganics. Additionally, an ammonium sulfate solution was analyzed with HPLC-ESIMS as an inorganic blank.

HSO_4^- , $\text{HSO}_4(\text{H}_2\text{SO}_4)^-$, and $\text{HSO}_4(\text{H}_2\text{SO}_4)_2^-$ were the dominant ions observed from the ammonium sulfate solution. These ion signals were subtracted from the SOA mass spectra to remove the remaining inorganic contribution. The mass analyzer was a high-resolution (100,000 $m/\Delta m$ at m/z 300) linear-ion-trap (LTQ) OrbitrapTM mass spectrometer (Thermo Corp.) operated in the negative ion mode with a mass range of 80-2000 m/z . The LTQ-Orbitrap was calibrated with commercial standard (LTQ ESI Negative Ion Calibration Solution, Thermo Scientific, Inc.) prior to mass spectral analyzes (mass accuracy up to 0.5 ppm at m/z 500).

C.3 Results and Discussion

C.3.1 Photooxidation of MPAN

Figure C.4a shows the reaction progress for a representative low-NO MPAN experiment under dry conditions. Reagents were equilibrated in the chamber prior to the initiation of photochemistry (yellow shaded region). Figure C.4b shows a representative low-NO MPAN experiment where α -pinene was added at the beginning of the reaction to scavenge NO_3 , and MAE was added at the end (after the reaction mixture has stabilized with lights off) to observe its effects on SOA formation.

A low yield of NO_2 ($7 \pm 3\%$) is observed by the NO_2/APN instrument and confirmed by the negligible CIMS PNA signal. This NO_2 formation is likely due to thermal decomposition of MPAN ($\tau_{288K} \sim 35$ h at the NO_x conditions in Expt. 2-3 Nouaime *et al.*, 1998; Roberts and Bertman, 1992) because a $10 \pm 5\%$ yield of PAN was also observed. The MPAN decomposition produces NO_2 and acylperoxyl radical, which is subsequently converted to the acyloxyl radical from reaction with either NO or HO_2 (Orlando *et al.*, 1999). The acyloxyl radical decarboxylates to the vinyl radical that ultimately forms PAN and other products through subsequent reactions (Chuong and Stevens, 2004). The thermal decomposition is calculated to be 10-25% of the total MPAN loss, qualitatively consistent with observed yields. The uncertainty is due to difficulty in determining the NO_2/NO ratio when NO_x is low. Neither PAN nor the NO_2 yield was enhanced in the presence of α -pinene (Figure C.4b), suggesting they both originate from MPAN. The lower bound (10%) of the MPAN decomposition is used to correct gaseous molar yields.

In contrast to NO_2 , the experiments performed with α -pinene conclusively demonstrate high yields of an NO_3 coproduct, as suggested by mechanisms 1 and 3 (Figure C.2). Figure C.5 shows that upon photooxidation of MPAN in the presence of α -pinene, PNP is formed in $\sim(35 \pm 17)\%$ yields with respect to α -pinene loss and

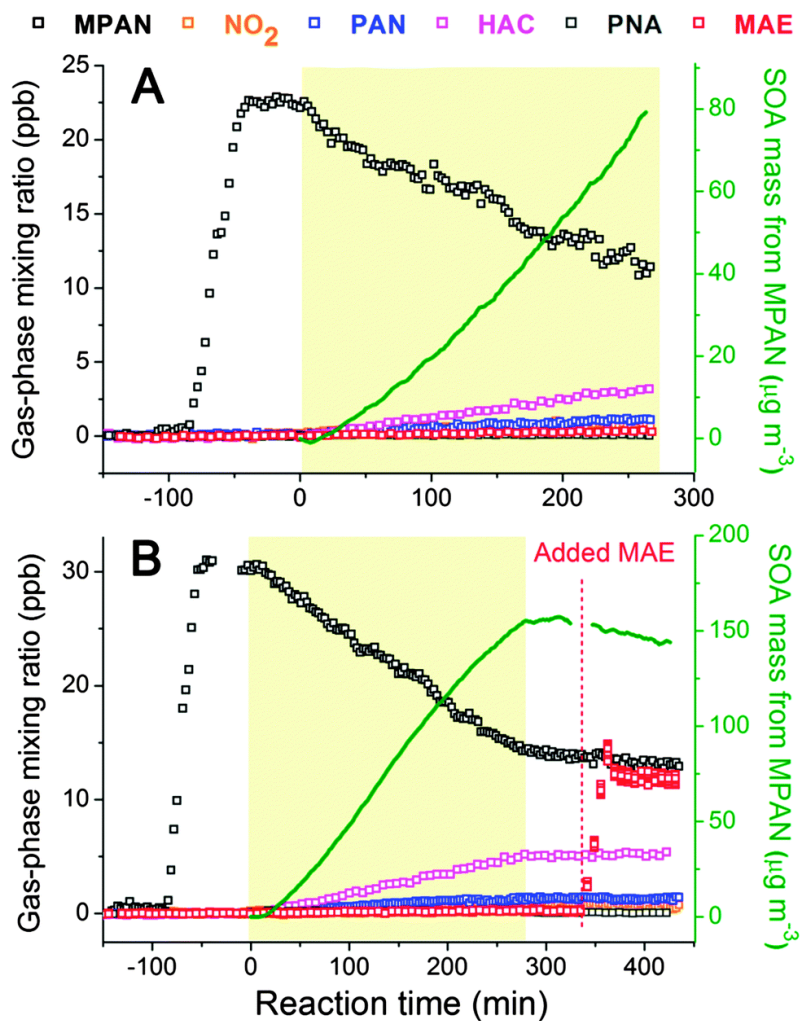


Figure C.4: Representative MPAN photooxidation experiments (A) performed with MPAN and H_2O_2 (Expt. 3, base experiment) and (B) the base experiment with the initial addition of α -pinene and subsequent injection of MAE standard (Expt. 4). The yellow shaded areas designate the time period when photochemistry occurs in each experiment. The right mass axis corresponds only to the SOA trace (green line).

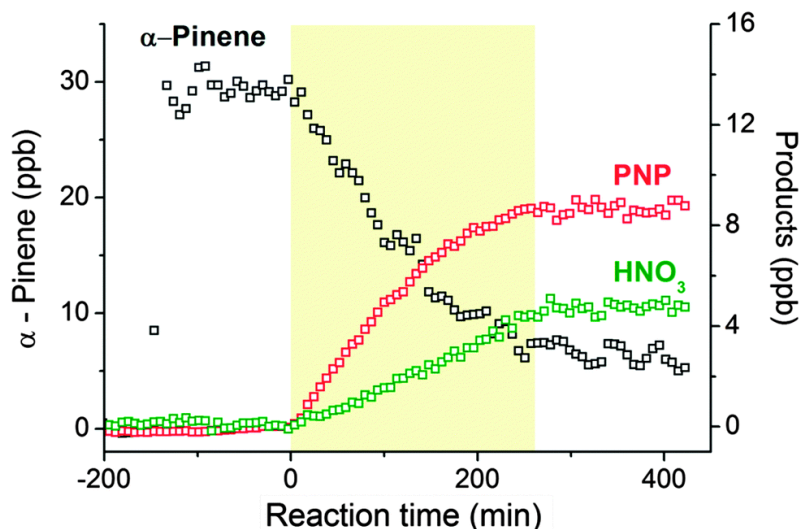


Figure C.5: Representative results from NO_3 scavenging experiment using α -pinene (Expt. 4). The yellow shaded area designates the time period when photochemistry occurs. Note the double-vertical scales.

$\sim(70 \pm 35)\%$ yield with respect to MPAN loss. Experiments without α -pinene did not produce interfering species at the mass used for quantification of PNP. Furthermore, experiments performed during the FIXCIT campaign (Expt. 10, 13 in Table 2 of that work (Nguyen *et al.*, 2014b)) with 30 ppbv of α -pinene demonstrate that PNP is not formed under low- NO photooxidation conditions, similar to those used to oxidize MPAN here (Figure C.13a in the Supporting Information). However, PNP is an abundant product when NO_3 is used as an oxidant while HO_2 is present in the chamber (Figure C.13b in the Supporting Information). Using known rate coefficients of α -pinene with NO_3 and OH (Atkinson *et al.*, 2006), we estimate the steady state NO_3 concentration in Expt. 4 (Table C.1) to be $6.5 \times 10^6 \text{ mol cm}^{-3}$. The steady state OH concentration ($\sim 1.5 \times 10^6 \text{ mol cm}^{-3}$), which is reproducible within 25% under identical oxidant precursor and light conditions, is derived from separate low- NO photolysis experiments using isoprene as a reference hydrocarbon (Nguyen *et al.*, 2014b). Thus, we estimate that the loss of α -pinene is $\sim 40\%$ by NO_3 and $\sim 60\%$ by OH . This is in relatively good agreement with the PNP yield from α -pinene assuming most of the pinene nitrooxy alkylperoxy radical reacts with HO_2 to form PNP.

HNO_3 formation in MPAN experiments (Figure C.5) occurs likely from the NO_3 -initiated H-abstraction of alkanes (*e.g.* tridecane from the introduction of MPAN) or other saturated compounds, as the reaction of NO_3 with α -pinene and MPAN

will result largely in addition rather than abstraction. Using the steady-state radical concentrations derived above and reaction rate coefficients from the literature (Canosa-Mas *et al.*, 1999b), we estimate <0.1% of the MPAN loss was due to reaction with NO₃ radicals. HNO₃ is observed in all MPAN photooxidation experiments due to the ubiquitous presence of the tridecane solvent, and no enhancement is observed in the presence of α -pinene. HNO₃ provides evidence of another 30 ± 9% NO₃ yield from MPAN, which taken together with PNP, suggests that MPAN efficiently yields NO₃ and a coproduct upon reaction with OH. The high NO₃ yield confirms one shared aspect of mechanisms 1 and 3 (Figure C.2) and, in combination with the low NO₂ observations, allows us to rule out mechanism 2 as a significant contributor to the MPAN photooxidation chemistry.

We observe a large mass yield of SOA from the dry MPAN + OH experiments (Figure C.4, green traces), suggesting that the MPAN photooxidation chemistry is efficient at forming SOA in the absence of NO_x. Approximately (125-145)% SOA by mass (with respect to MPAN mass reacted) is formed, and assuming an average molecular weight of 340 g mol⁻¹ (the intensity-weighted average of the MPAN + OH high-resolution mass spectrometry data, assuming similar ESIMS sensitivities for observed analytes), approximately ~ (60 +15/-5)% by mole. The uncertainty is derived from corrections (*e.g.* for tridecane-derived SOA, particle wall loss, and MPAN thermal decomposition) and analysis of the average molecular weight of the SOA. The observation that SOA formation from MPAN + OH is not NO-dependent is consistent with the suggestion in mechanisms 1 and 3 (Figure C.2) that the traditional RO₂ chemistry of the thermalized radical A does not come into play. However, we note the data do not eliminate the possibility that an RO₂ formed after O₂ addition also rapidly decomposes to the same products.

Importantly, the SOA formation from MPAN + OH is prompt and occurs without the injection of inorganic seed aerosols. It is possible the SOA forms *via* nucleation (*e.g.* from the chemistry of larger VOC like tridecane) or growth in the presence of pre-existing seed particles that are under the size detection limit of the SMPS and AMS. Even if SOA growth occurs on dry, pre-existing, nanoparticles, most of the SOA formation occurs on primarily-organic particles after the first few condensation cycles. This observation favors the proposed mechanism 3 over mechanism 1 due to the need for MAE to undergo reactive uptake partitioning, which is a slow process for this compound even in the presence of hydrated, acidic sulfate particles that would accelerate ring-opening of the epoxide ($\gamma \sim 5 \times 10^{-4}$ when seed aerosols are

50% H₂SO₄ by mass) (Riedel *et al.*, 2015).

Of the putative SOA precursors, MAE is the only compound that has been detected by mass spectrometry due to its chemical stability. Throughout all experiments, we observed small to negligible yields of MAE in the gas phase ($2 \pm 1\%$, upper limit, see Experimental), whether the precursor was MPAN or MACR. FIXCIT experiments of MACR under low-NO conditions also did not observe any appreciable MAE production (Nguyen *et al.*, 2014b). Lin *et al.* (2013b) similarly observed a small gas-phase yield of MAE ($\sim 1\%$ from MACR, Figure S1 of that work), but suggested that MAE is so rapidly converted to SOA mass that most of it is observed in the condensed phase. Under the assumption that (50-80)% of MAE is observed as SOA, they estimated MAE yields are 18-32% from MPAN. We demonstrate that MAE is not well-converted to SOA and, in particular, not *via* the mechanism that forms the dominantly-organic particles in the MPAN experiments. It instead appears that MAE is a remarkably stable and volatile gas-phase species, with similar volatility to MPAN, which by itself does not form SOA through equilibrium partitioning. Notably, when $\sim(12 \pm 50)\%$ ppbv of MAE is injected into the chamber following the reaction period (Figure C.4b), no change to particle size or mass concentration can be observed.

To further evaluate the inertness of MAE, we injected a few hundred ppbv of MAE into a clean 1000 L Teflon bag alongside 500 ppbv of HNO₃ (~ 300 ppbv of which remained in the gas phase, and the rest, presumably, coated the chamber walls). No observable wall loss of MAE occurred over the course of 2.5 h (Figure C.14 in the Supporting Information); this is identical to its behavior in the absence of acid. It appears that the small quantity of MAE formed from MACR oxidation is not an eager participant in the surface- and/or water-induced partitioning that often leads to SOA formation. The inertness we observe provides insight into why 300 ppbv ($\sim 1250 \mu\text{g m}^{-3}$) of MAE produced only $\sim 10 \mu\text{g m}^{-3}$ of SOA through reactive uptake in the Lin *et al.* (2013b) work, even when using seed particles that are exceptionally acidic (~ 50 wt% H₂SO₄ at RH < 10%). The evidence suggests that the low (<2%) gas-phase mixing ratios observed in this work and by Lin *et al.* (2013b) (from MACR) indeed represent a measure of the entire yield of MAE. Thus, it appears that the disagreement between this work and that of Lin *et al.* (2013b) lies in the assumption of MAE's ability to form SOA, and not in the observations of MAE itself. As MAE formation is negligible both from MPAN and MACR, mechanism 1 is ruled out as a significant contributor to MPAN-derived SOA.

A key element to understanding the MPAN + OH reaction lies in the measurement of hydroxyacetone (HAC). The HAC yield determined here ($\sim 25 \pm 7\%$) is consistent with the upper limit determined by Orlando *et al.* (2002) ($< 40\%$), but more than a factor of two lower than the yield determined by Grosjean *et al.* (1993c) ($\sim 60\%$). Both of the previous works were performed under high-NO conditions using ethyl nitrite as an OH precursor. The source of discrepancy with regards to the Grosjean work is not clear; however, a similar trend in data agreement can be observed in the determination of rate coefficients of OH + MPAN. We measured $k_{288K} \sim 3 (\pm 1) \times 10^{-11} \text{ cm}^3 \text{ mol}^{-1} \text{ s}^{-1}$, which compares well with Orlando *et al.* (2002) ($k_{277K} \sim 3.2 (\pm 0.8) \times 10^{-11} \text{ cm}^3 \text{ mol}^{-1} \text{ s}^{-1}$), but is an order of magnitude higher than the value reported by Grosjean *et al.* (1993c) ($k_{298K} \sim 3.6 (\pm 0.4) \times 10^{-12} \text{ cm}^3 \text{ mol}^{-1} \text{ s}^{-1}$). The coefficient by Orlando *et al.* (2002) is preferred by IUPAC due to its consistency with the OH reaction with structurally similar APNs, and our data is in agreement with this recommendation (Atkinson *et al.*, 2006; Saunders *et al.*, 1994). Thus, we only consider the comparison between this work and that of Orlando *et al.* (2002).

If the production of HAC occurs *via* the lactone-production pathway (as the data seem to indicate) then the yield would be independent of NO mixing ratio. The agreement in the HAC yield obtained under low-NO conditions (this work) and high-NO conditions (Orlando *et al.*, 2002) suggests that HAC is not formed from the alkylperoxy radical B in the MPAN + OH reaction. Finally, the experimentally-determined HAC yield (and, consequently the remainder HMML yield) is comparable to those theoretically predicted by Kjaergaard *et al.* (2012) ($\sim 36\%$ of HAC). In contrast, Lin *et al.* (2013b) suggest a low HAC yield ($\sim 3\%$). The current work cannot differentiate the 2% of thermalized radical A that is predicted to form (Kjaergaard *et al.*, 2012), ultimately generating the alkoxy radical under high NO_x conditions, because the products would likely include HAC and NO_3 . Together, the experimental data support the HMML mechanism from the MPAN + OH reaction. We estimate approximately 25% of the reaction yields HAC + CO + NO_3 and 75% of the reaction yields HMML + NO_3 , with 75-100% of HMML leading to the formation of SOA under dry conditions.

To investigate whether there is a route to HMML from thermalized alkyl radicals, we performed experiments with saturated APNs that are analogous to MPAN. The photooxidation of the saturated analogues occurs *via* H-abstraction instead of OH-addition, which generates lower-energy alkyl radicals. For example, we synthesized A in the chamber *via* the OH-initiated photochemistry of 3-hydroxy-

2-methylpropanoyl peroxyxynitrate (HMPPN). HMPPN is a major product of the high-NO₂ OH-initiated oxidation of hydroxymethyl propanal (HMP), which was produced by dark ozonolysis of 23IMBO (Section C.5 and Figures C.15 and C.16a in the Supporting Information). Expected gas-phase products arising from RO₂ and RO radicals were observed from the chemistry of A but not A* (Figure C.17 in the Supporting Information), *e.g.* the hydroxynitrate, the hydroxyhydroperoxide, hydroxyacetone, and 2-oxopropanoyl peroxyxynitrate (Orlando *et al.*, 2002). Qualitatively compared to MACR, the SOA formation from the photochemistry of HMP (Expt. 11, Figure C.16b in the Supporting Information) and isobutyraldehyde (Expt. 10, not shown) is negligible ($\ll 1\%$). Chan *et al.* (2010a) first suggested the importance of the β -unsaturation in MPAN, following the observation that α,β -unsaturated aldehydes produced the largest SOA yields. Our results are consistent with their explanation.

Additionally, we use the potential energy surfaces from the Kjaergaard *et al.* (2012) work to calculate the relative fates of A. Compared to a typical effective rate for the reaction of alkyl radicals with O₂ at 1 atm air (O₂ = 21%) and 298 K ($k_{eff} \sim 1 \times 10^7 \text{ s}^{-1}$), the thermalized unimolecular decomposition of A to HMML is much slower ($k_{A \rightarrow HMML} < 10^3 \text{ s}^{-1}$). This translates to a calculated 0% yield of HMML in the HMPPN + OH reaction (100% reacts with O₂). In comparison, Kjaergaard *et al.* (2012) estimated the decomposition of A* to HMML is fast under the conditions they studied ($k_{A^* \rightarrow HMML} \sim 4 \times 10^9 \text{ s}^{-1}$), translating to a 61-74% HMML yield from MPAN (2% is stabilized to A). The theoretical-derived kinetic results are consistent with observations for these C₄ APN-derived alkyl radicals.

Figure C.6 summarizes the chemical mechanisms in the OH-initiated oxidation of MPAN and HMPPN to reflect the current scientific knowledge. It is also possible that larger APNs behave differently than the C₄ APNs discussed here. For example, it is not clear if APNs from the monoterpene aldehydes such as pinonaldehyde (saturated) and limonaldehyde (unsaturated, in the gamma position) are able to produce SOA or undergo a different photochemical fate. These larger APN systems are intriguing because they can be produced in the laboratory but have not been observed in the ambient atmosphere (Nguyen *et al.*, 2014b).

C.3.2 Atmospheric Fate of HMML

To study the SOA formation from HMML under conditions more relevant to the atmosphere, we performed MACR high-NO₂ photooxidation experiments with

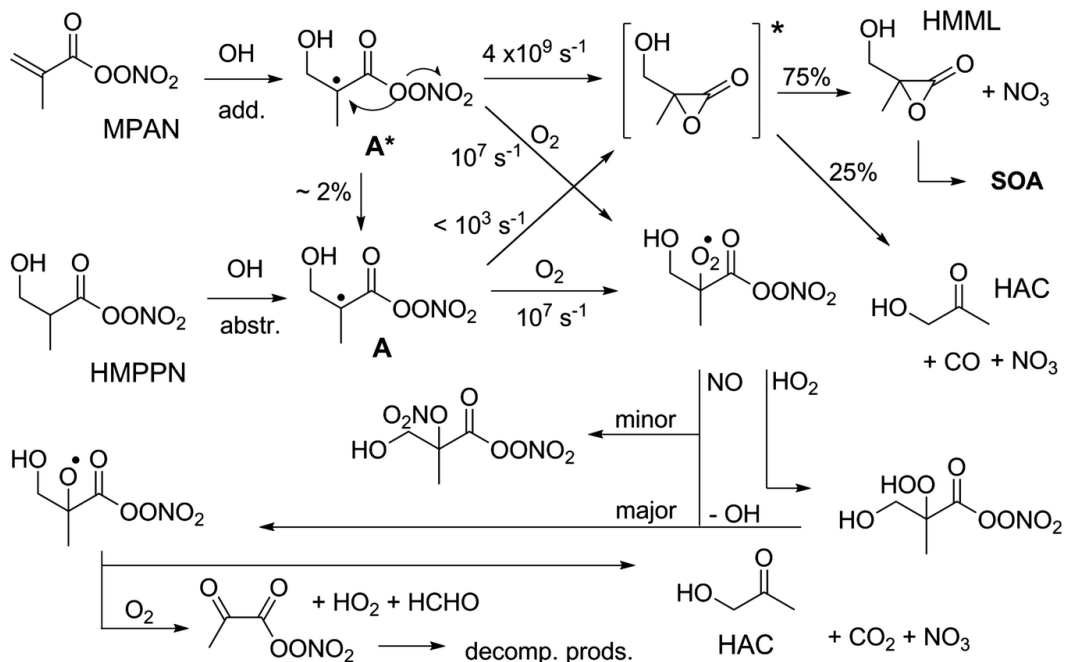


Figure C.6: The OH-initiated oxidation mechanism of MPAN and HMPPN derived from the low-RH experiments conducted in this work. The HMML formation from MPAN arises from a chemically-activated mechanism while the product formation from HMPPN arises from a thermalized alkyl radical + O_2 reaction.

hydrated ammonium sulfate (AS) seed particles at 40% and 85% RH (efflorescence and deliquescence RH of AS are $\sim 30\%$ and $\sim 80\%$, respectively) (Biskos *et al.*, 2006). Figure C.7 shows that the SOA production is lower and gas-phase 2MGA yields are higher when the reaction occurs in deliquesced AS particles (Expt. 13, liquid water $\sim 75 \text{ vol}\%$) compared to primarily organic particles (under dry conditions, Expt. 9). The small MAE signal did not increase under humid conditions, suggesting that the formation of this compound is likely not important in the ambient environment. The production of HAC is observed to slightly increase toward the end of the experiment. However, this change is within the uncertainty of the HAC determination ($\pm 30\%$). If the difference in HAC signal between dry and humid is real, the underlying mechanism is unclear. The systematic uncertainty in calculating mixing ratio for 2MGA is approximately $\pm 50\%$. However, if all of the $\sim 12\text{-}13 \text{ ppb}$ of 2MGA in the gas phase is converted to particle mass, the volatilization of 2MGA may explain almost 100% of the $\sim 60 \mu\text{g m}^{-3}$ SOA mass discrepancy between the two experiments. 2MGA is typically used as a tracer for isoprene SOA; however, it appears that its accommodation in the condensed phase is low at typical aerosol-phase pH. Recent observations in the Southeast U.S. and Amazon forests support the

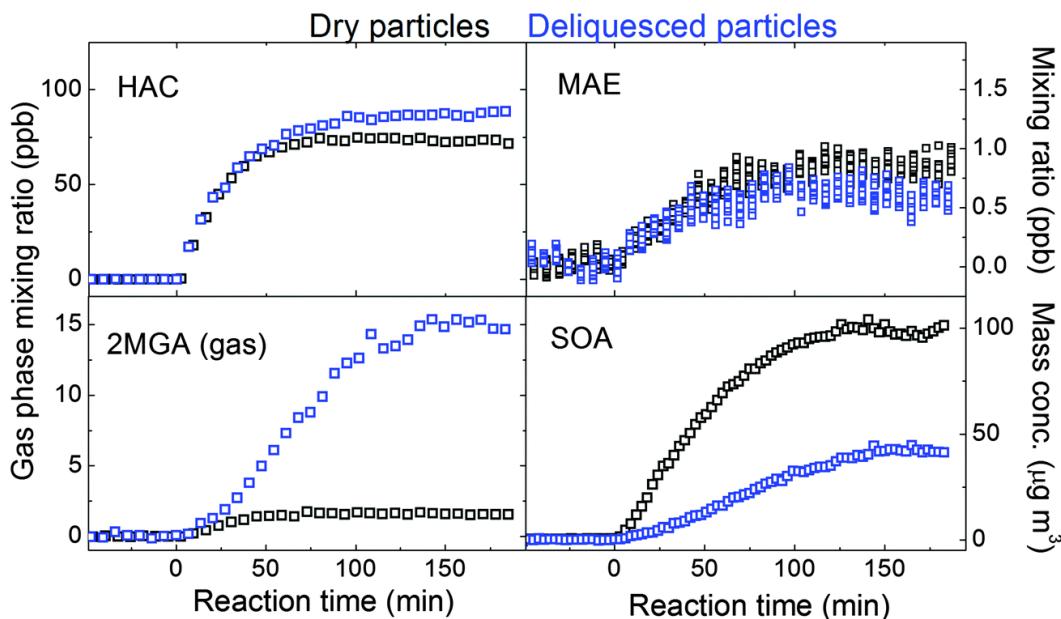


Figure C.7: The formation of gas-phase species and secondary organic aerosols under dry conditions (black markers) and under humid conditions (85% RH) with deliquesced ammonium sulfate seeds (blue markers).

idea that 2MGA may exist primarily in the gas phase in humid biogenic environments (Isaacman-VanWertz, 2014).

Figure C.8a shows the CIMS gas-phase measurement of 2MGA (from a 0.075 M solution of the synthesized standard) as the solution is increasingly acidified. 2MGA behaves similarly to a semivolatile compound such as isoprene epoxydiol in the CIMS instrument, *i.e.* it takes approximately 10 minutes to equilibrate with Teflon tubing compared to a more-volatile compound such as hydroxyacetone (<1 min). The gas-phase mixing ratio linearly increases with decreasing solution pH (Figure C.8b) in the measurement range, as expected for a semi-volatile organic acid. This pH-dependent volatilization is likely to be important for understanding the SOA formation from not only MPAN oxidation, but other types of atmospheric reactions that produce organic acids in the condensed phase, *e.g.* cloud-processing oxidation (Carlton *et al.*, 2006; Sorooshian *et al.*, 2007), ozonolysis of alkenes (Christoffersen *et al.*, 1998; Koch *et al.*, 2000), and other reactions.

Interestingly, gas-phase 2MGA is not significantly enhanced and aerosol mass is not significantly decreased in the 40% RH experiment (Expt. 12) compared to the dry experiments. It is possible that the liquid water content under these conditions (~30 vol%) is not high enough to dominate the reaction with HMML

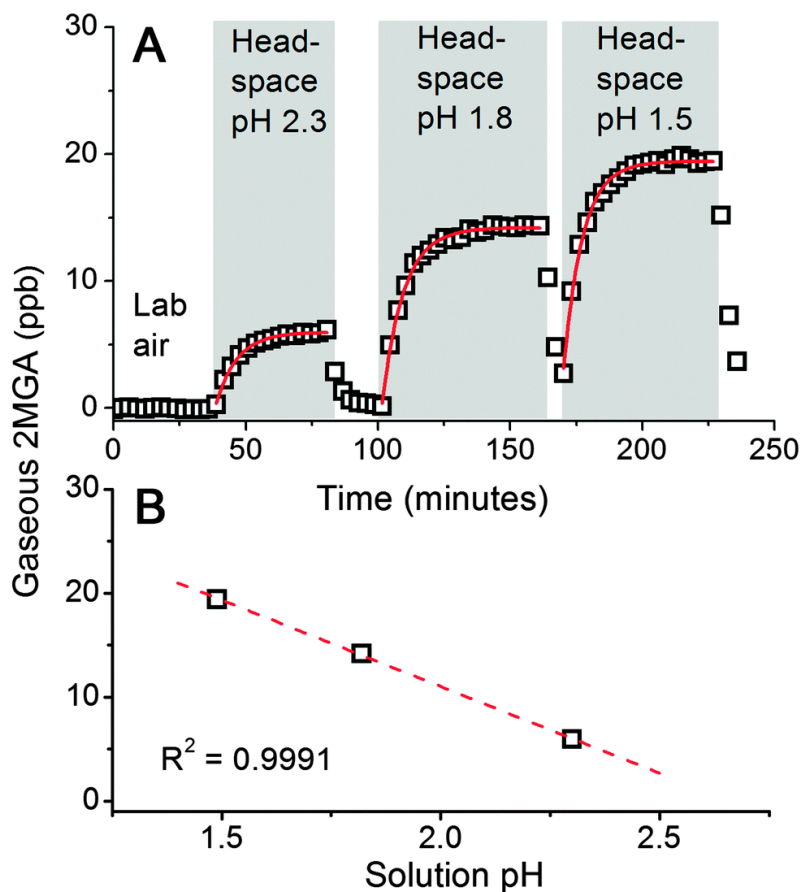


Figure C.8: CIMS measurements of the headspace air above a 0.075 M 2-methylglyceric acid (2MGA) solution: (A) the gaseous 2MGA signal when switching from lab air to solutions with different pH and (B) the headspace 2MGA mixing ratio (obtained through exponential fitting) is a linear function of pH in the measurement range.

or there is a barrier to 2MGA volatilization. For example, if organic-inorganic phase separation occurs at RH between efflorescence and deliquescence (Bertram *et al.*, 2011; O'Brien *et al.*, 2015), the reaction of gas-phase HMML with water and solvated ions and the volatilization of aqueous 2MGA may be hindered by an organic shell. Additionally, when liquid water content is lower (and thus, ionic strength is higher), organic acids such as 2MGA may form involatile salts with NH_4^+ and other cations (Wang and Laskin, 2014). Salt formation is not expected to be significant for deliquesced particles, but can be considerably enhanced for drier metastable particles at 30-50% RH (Laskin *et al.*, 2012).

Figure C.9 shows the results of high-resolution mass spectrometry (HR-MS) analyzes of SOA collected from MPAN and MACR photooxidation. When the

photooxidation of MACR is performed without inorganic seeds and under dry conditions, long oligomer families of 2MGA that are separated by 102.0317 Da (the exact mass of HMML) are observed, consistent with earlier mass spectrometry observations (Nguyen *et al.*, 2011b; Surratt *et al.*, 2006; Szmigielski *et al.*, 2007). The SOA composition from MPAN + OH appears almost identical to that of MACR + OH + NO₂. In addition to the 2MGA + HMML oligomers, the MACR high-NO_x photooxidation produces an organic nitrogen oligomer family (Figure C.9, blue peaks). The organic nitrogen family of 2MGA-nitrate + HMML elutes primarily at later retention times (8-20 min), likely due to their lower polarity compared to organic sulfates and acids, but is absent in other chemical systems, including the MPAN + OH low-NO_x reaction. These N-containing SOA compounds are likely formed from the reaction of HNO₃ (from NO₂ + OH reaction in the MACR high-NO_x experiments) with HMML in the condensed phase or interfacial region, which generate the nitrate ester of 2MGA through nucleophilic ring opening.

When aqueous sulfate is present, the sulfate ester of 2MGA is produced (Figure C.9, magenta peaks), which react with HMML similarly to 2MGA and 2MGA-nitrate. In ammonium sulfate particles at 40% RH, the oligomer families of 2MGA-sulfate + *n*(HMML) and 2MGA + *n*(HMML) are observed up to the trimer and dimer, respectively. In the deliquesced AS seeds at 85% RH, the monomer compounds 2MGA, 2MGA-sulfate, and the sulfate nitrate (C₄H₆O₉NS⁻ ion) dominate the mass spectra. An exception is the dimer 2MGA-nitrate + HMML that has higher signal than the monomer. This may be attributed to the fact that nitrate ion is a poor nucleophile and nucleophilic substitution with water and sulfate may readily occur, so the monomer nitrate has a short condensed-phase lifetime. Thus, the organonitrate may be more stable in the dimer form. However, it is also possible the nitrate dimer is more ionizable in negative mode ESI compared to the monomer. We do not expect a large ionization difference between 2MGA-nitrate and 2MGA as the carboxyl moiety is believed to be the charge carrier for this compound in negative mode ESI with aqueous-based solvents (Yamashita and Fenn, 1984). The combined mass of the SOA from these organic acid and hetero-atom compounds in the 85% RH experiment, however, is lower than the mass of 2MGA in the gas phase (Figure C.7).

These aerosol phase HR-MS observations are consistent with earlier suggestions that relative humidity plays a role in modifying the composition and yield of isoprene-derived high-NO_x SOA (Nguyen *et al.*, 2011a; Zhang *et al.*, 2011). However, previous works did not study 2MGA particle/gas partitioning and discussions were

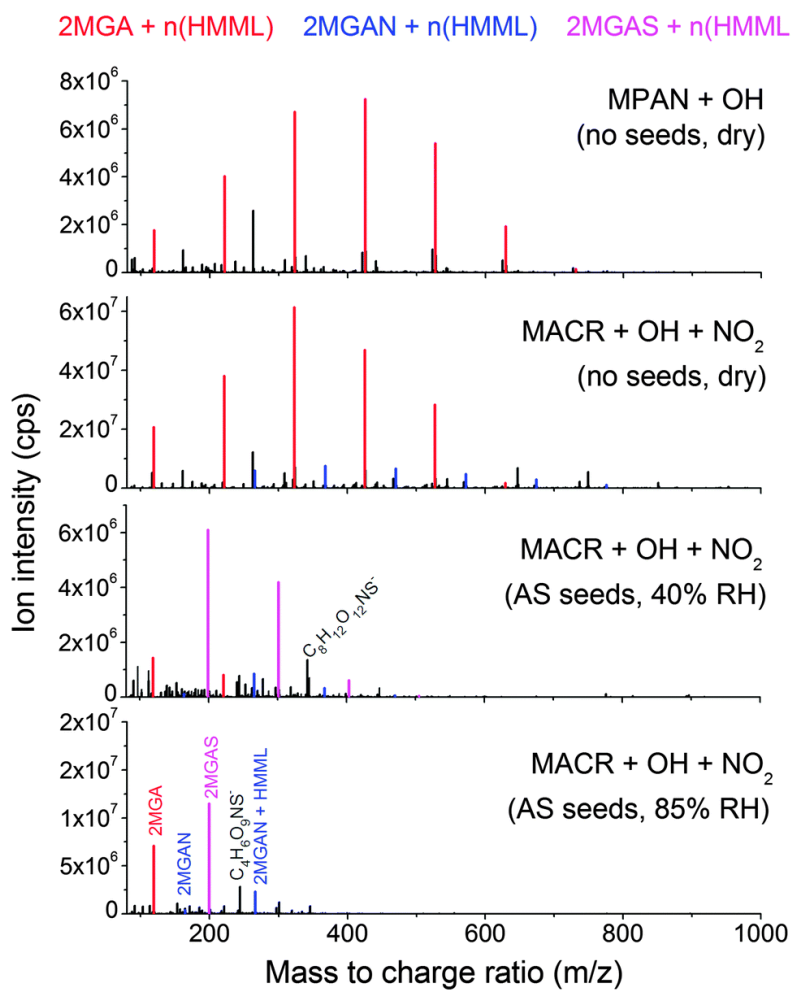


Figure C.9: Negative mode ESI-HRMS analysis of select SOA samples, integrated for retention times 2.5-3.5 min. The inorganic constituents have been separated by HPLC. Oligomer families comprised of HMML units are color-coded based on the monomer compounds (2MGA = 2-methylglyceric acid, 2MGAN = 2-methylglyceric acid nitrate, and 2MGAS = 2-methylglyceric acid sulfate).

framed with respect to poly-condensation reactions (*e.g.* a Fisher type esterification) – a hypothesis that is not consistent with the present data. Furthermore, it has been recently shown that Fisher type esterification is too slow to form 2MGA oligomers under standard conditions (Birdsall *et al.*, 2013). This does not, however, preclude condensation reactions from occurring when aerosol particles or cloud/fog droplets are evaporated (De Haan *et al.*, 2011; Nguyen *et al.*, 2012). In light of the gas-phase mechanism of MPAN + OH presented here, the molecular driving force behind the effect of RH on MPAN aerosol composition and yield can now be understood in terms of lactone polymerization.

Figure C.10 shows the proposed mechanism with which HMML is converted to SOA and gas-phase 2MGA. Lactones are well-known to produce polyesters *via* polyaddition (Löfgren *et al.*, 1995). We suspect that, in nature, the anionic ring opening polymerization scheme is the active mechanism. Nucleophilic attack at the sp^3 carbon is dominant for α -lactones (Greenberg and Liebman, 1978), partly due to the stability of the carboxylate (estimated to be only ~ 10 kcal mol $^{-1}$ higher in energy than the α -lactone) (Liebman and Greenberg, 1974). The propagated carboxylate can repeatedly add HMML under low RH conditions, where its main fate is reaction with organics that coat the particle. In ambient SOA, ring-opening initiators may be aqueous inorganic anions or myriad carboxylates that are present in the condensed phase. When liquid water is in excess (as is mainly the case in the lower troposphere), it appears the main fate of HMML is reaction with H $_2$ O, aqueous sulfate, or aqueous nitrate, and not with organics. Because the organonitrate is more easily hydrolyzed, the major product of the reaction under typical atmospheric conditions is expected to be monomeric 2MGA and 2MGA sulfate. The 2MGA may re-partition into the gas phase, leading to significantly reduced SOA mass yields.

C.4 Atmospheric Implications

The representation of MPAN oxidation in atmospheric models has important ramifications. Thus far, only the proposed MAE mechanism (*i.e.* reactive uptake) has been considered for modelling SOA formation and framing field observations (Pye *et al.*, 2013; Worton *et al.*, 2013). Previously modelled SOA formation from MAE increases with particle acidity, while simulations based on HMML are expected to exhibit a different temporal and spatial variability. Pye *et al.* (2013) used the HMML and MAE yields suggested by Lin *et al.* (2013b) (57% and 21%, respectively); however, both compounds were assigned to have the acid-catalysed heterogeneous fate of MAE (*i.e.* essentially converting HMML mass to MAE). The observed and

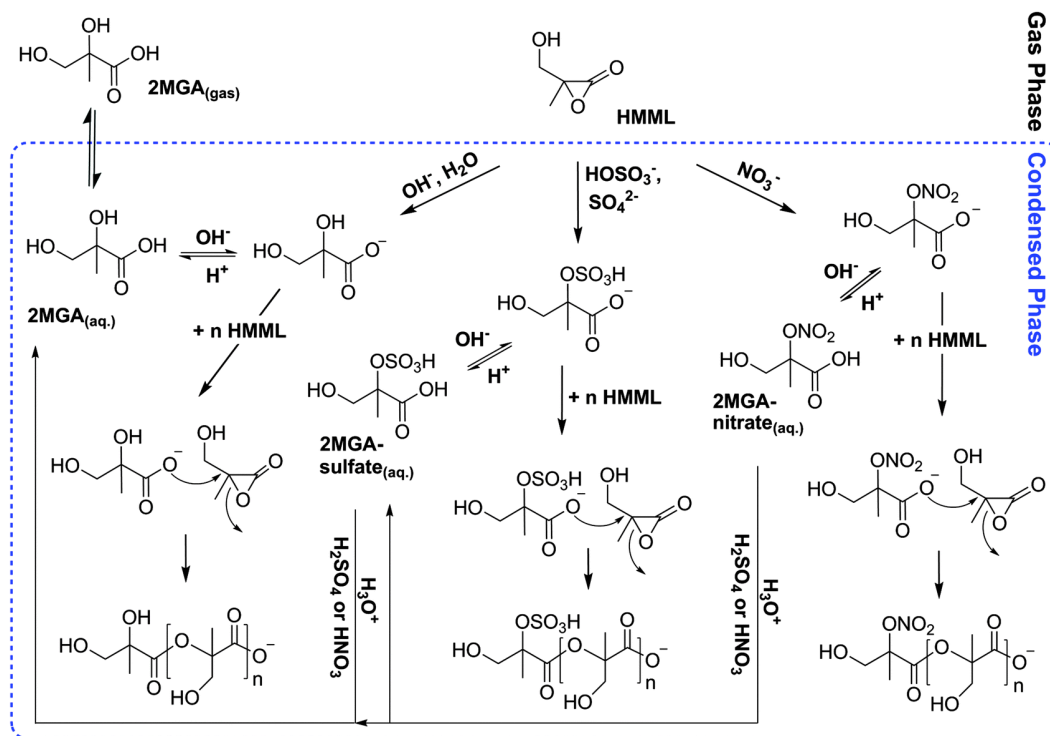


Figure C.10: Mechanism of SOA production from HMML (the blue dashed area represents the condensed phase). When particle liquid water is high, the main fate of HMML is reaction with water to produce monomeric 2MGA or sulfate and nitrate ions to produce 2MGA-sulfate and 2MGA-nitrate, respectively. The 2MGA monomer is volatile enough to re-partition to the gas phase. When the SOA composition is higher in organics than water, the main fate of HMML is reaction with its condensed-phase derivatives, producing low-volatility polyesters that increase SOA mass. Hydrated particles with higher free acidity may favour the monomeric form of 2MGA by neutralizing the carboxylate and hydrolyzing the sulfate and nitrate esters, possibly suppressing SOA growth.

predicted SOA from MPAN deviates from the 1:1 relationship in that work, likely a result of the assumed SOA mechanism. Figure C.8 and the mechanisms in Figure C.10 suggest a more complex impact of particle free acidity. For example, in conditions when particle free acidity is high, the neutral form of 2MGA will be favored and the organosulfate/organonitrate may hydrolyze more rapidly (Hu *et al.*, 2011). Both situations will enhance the abundance of 2MGA in the gas phase at the expense of lower-volatility derivatives that are important for SOA formation and growth.

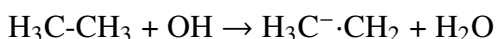
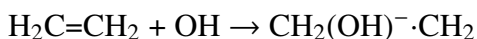
The regional atmospheric importance of MPAN will vary with NO_2/NO ratio and isoprene emissions. Kjaergaard *et al.* (2012) estimated that approximately 4 Tg of HMML is produced per year (up to $0.8 \mu\text{g m}^{-3} \text{ day}^{-1}$ in the Southeast

U.S.). However, whether the carbon from HMML is directed toward the formation of gaseous 2MGA or SOA will depend on atmospheric conditions and particulate matter characteristics. Typically, oligomers are not observed in ambient SOA and the mass concentrations of 2MGA and 2MGA-sulfate are low (*e.g.* 7-9 ng m⁻³ and 12 ng m⁻³ in Southeast U.S., respectively) (Lin *et al.*, 2013a). The low ambient observations in the Southeast US, a region characterized by higher particle liquid water and lower particle pH (Guo *et al.*, 2015; Nguyen *et al.*, 2014c), are consistent with the HMML-derived SOA formation mechanism (Figure C.10). This work demonstrates that certain "SOA tracers" have more complex fates in nature than previously recognized. Interpreting the abundance of aqueous 2MGA and 2MGA-sulfate will require knowledge of physical parameters that may not be available for these compounds (*e.g.* Henry's Law coefficients, reaction coefficients, temperature and pH-dependent accommodation). We expect that integrating the lactone mechanism into atmospheric models will produce a more accurate representation of the magnitude, temporal variation, and spatial distribution of isoprene-derived organic compounds (whether in the gas or condensed phase) near anthropogenically influenced regions.

C.5 Supporting Information

C.5.1 Photooxidation of Saturated Analogues of MPAN

Lactone formation has been suggested only for APNs of aldehydes with a β -alkenyl moiety, MACR and acrolein (Kjaergaard *et al.*, 2012). Here, we investigate the extent to which saturated APNs may access a similar reaction pathway. The OH-initiated oxidation of saturated and unsaturated compounds proceeds predominantly through abstraction and addition channels, respectively, illustrated here for ethylene and ethane:



The abstraction-generated alkyl radical is less energetic than the alkyl radical formed *via* addition of OH. It is unclear whether most of the abstraction radicals would be collisionally stabilized or if the $-\text{C}(\text{O})\text{OONO}_2$ neighboring group enhances its decomposition. To investigate the effects of alkyl radical energetics, we conducted additional experiments using radicals A and C (Figure C.6) that are analogous to A*. The radical A (produced in Expt. 11) is the thermalized version of A*, given its formation mechanism; and C (produced in Expt. 10) is structurally similar to A, but missing the hydroxyl group. As the results of both experiments are consistent, we limit the discussion only to the chemistry of A, a third-generation oxidation intermediate of 2-methylbut-3-ene-1-ol (231MBO).

Figure C.16a in the Supporting Information shows the formation of the 3-hydroxy-2-methylpropanoyl peroxyxynitrate (HMPPN) from a chamber experiment. HMPPN is the precursor of A from 231MBO, formed in a synthetic scheme that involves ~21 h of dark ozonolysis chemistry (to react away most of the C=C bonds of 231MBO) followed by a shorter phase of high-NO₂ photooxidation. Ozonolysis of 231MBO produces the aldehyde hydroxymethyl propanal (HMP) in high yield alongside the simplest Criegee (CH₂OO), which is observed by CIMS as its bimolecular product with water, hydroxymethylhydroperoxide (not shown) (Neeb *et al.*, 1997). The ozonolysis period (performed without an OH scavenger) produced a small yield of SOA (<3%) that has the same temporal behavior as HMP. After the stabilization of the dark gas-phase mixture, NO₂ and methyl nitrite were injected and the near-UV lamps were switched on to initiate the OH-oxidation chemistry in the presence of NO₂. The slight decay of HMP prior to initiation of photochemistry (*e.g.* starting at -20 min, Figure C.7b) is due to reaction with NO₃, formed after the injection of NO₂ through its reaction with O₃; however, this slower chemistry is promptly overtaken by the OH oxidation that occurred in the photolytic period.

The photochemistry of HMP (and that of HMPPN) does not produce additional SOA (Figure C.16b in the Supporting Information, $\ll 1\%$ SOA yield from HMP). In comparison, when MACR is oxidized in a similar manner (Figure C.16c in the Supporting Information), SOA is observed to grow after a ~ 15 min delay. A delay in observing SOA is fairly typical when seed particles are not used (Figure C.4) because the lower threshold for particle diameter in this work is 20 nm. Additionally, the SOA should be second-generation so the observed delay may encompass a chemical delay. As HMP and MACR both produce the APNs, which upon oxidation form structurally identical alkyl radicals, the results suggest that the difference in excess energy of A and A* is responsible for the disparate SOA formation behaviour.

Experimental evidence for HMPPN reaction and A + O₂ reaction can be provided by the CIMS observations of alkylperoxyl radical (RO₂) and alkoxy radical (RO) reaction products (Figure C.17 in the Supporting Information; see Figure C.6 in the main text for the mechanism). During the photolytic period, we observed the minor products of the RO₂ + NO reaction channel, the hydroxynitrates (RO₂ + NO \rightarrow RONO₂) and the major product of the RO₂ + HO₂ reaction channel, the hydroxyhydroperoxides (RO₂ + HO₂ \rightarrow ROOH + O₂) from the HMPPN + OH reaction. These radical termination products have low volatility (*e.g.* the hydroperoxide has a molecular formula of C₄H₇NO₈) in addition to low yields, resulting in low analyte signals in the CIMS. We also observed the major products from the high-NO reaction (RO₂ + NO \rightarrow RO + NO₂ \rightarrow decomposition products), which include HAC ($\sim 25\%$ from HMP) and the APN of pyruvaldehyde (2-oxopropanoyl peroxyxynitrate (2OPN), $< 1\%$ from HMP, green trace in Figure C.17 in the Supporting Information) (Orlando *et al.*, 2002). The relative yields of HAC is 3 - 30 times higher compared to the 2OPN when estimated from HMPPN; however the absolute yields are not available as the amount of HMPPN reacted is unknown. The disparity in relative yields may be due to the expected propensity for 2OPN to decompose (*via* the NO₂ and NO₃ channels) compared to the high stability of HAC (Orlando *et al.*, 2002). The formation of RO₂ radical termination products and RO decomposition products in the MPAN + OH reaction was negligible (Figure C.17a in the Supporting Information). The HAC formation in the MPAN + OH reaction is *via* HMML decomposition. Together with SOA data and HMPPN-derived product observations, the RO₂ reaction products provides a consistent picture of predominantly HMML formation from MPAN + OH and RO₂ formation from HMPPN + OH.

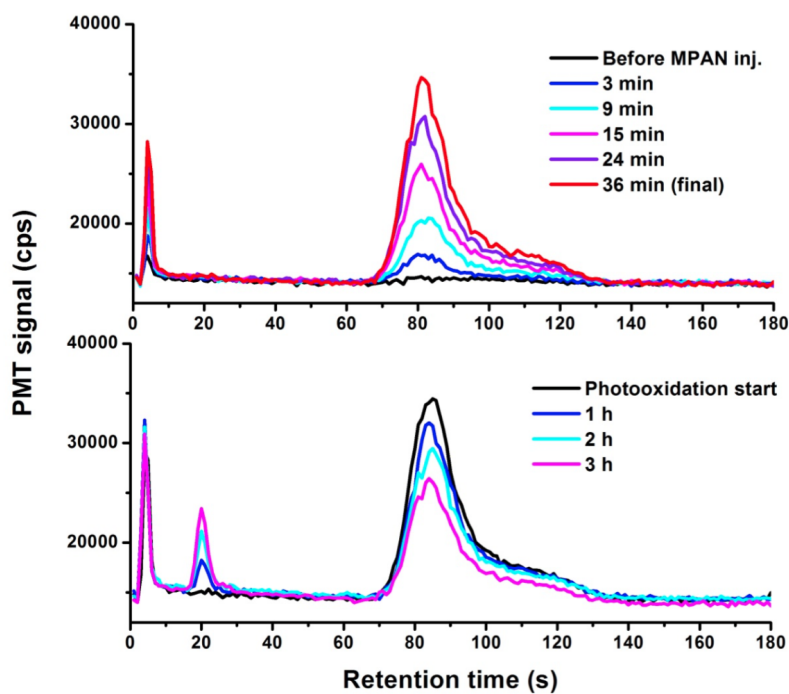


Figure C.11: Chromatograms of NO₂, PAN, and MPAN in the NO₂/APN analyzer (retention times 10, 20, and 80 s, respectively). Top panel: signals from NO₂ and MPAN are observed when introducing MPAN into the chamber due to a small decomposition yield of MPAN in room-temperature Teflon lines. This decomposition is not observed in the headspace of pure MPAN in tridecane when the standard is kept cold and the sampling line is short (< 0.3 m). Bottom panel: photooxidation of MPAN over the course of 3 h, when the MPAN signal decreases and PAN is observed to form. The NO₂ signal does not change significantly, possibly due to the compensating effects of decreasing signal from MPAN and increasing signal from other sources.

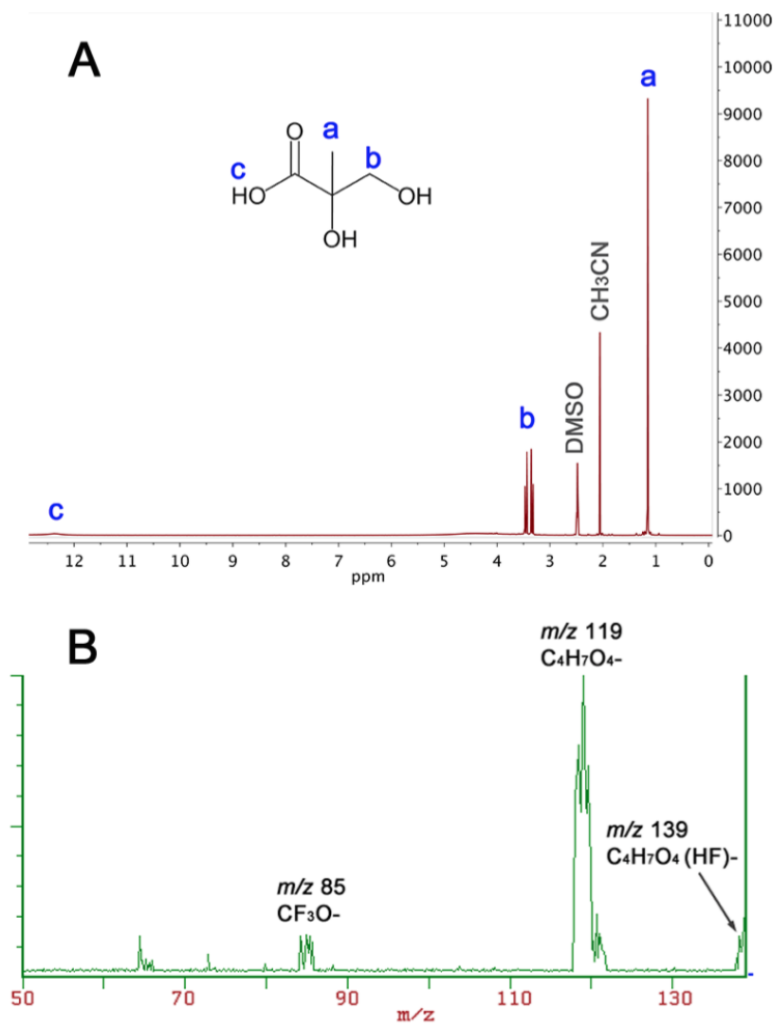


Figure C.12: Characterization of 2-methylglyceric acid with proton NMR using DMSO solvent, the semi-pure mixture (containing 7% acetonitrile) was further purified through crystallization and B: tandem mass spectrometry (MS/MS) with triple quadrupole CIMS, the 2-methylglyceric acid is observed only as its fluoride transfer ion with CF_3O^- and collision-induced dissociation leads primarily to the deprotonated compound ($\text{C}_4\text{H}_7\text{O}_4^-$).

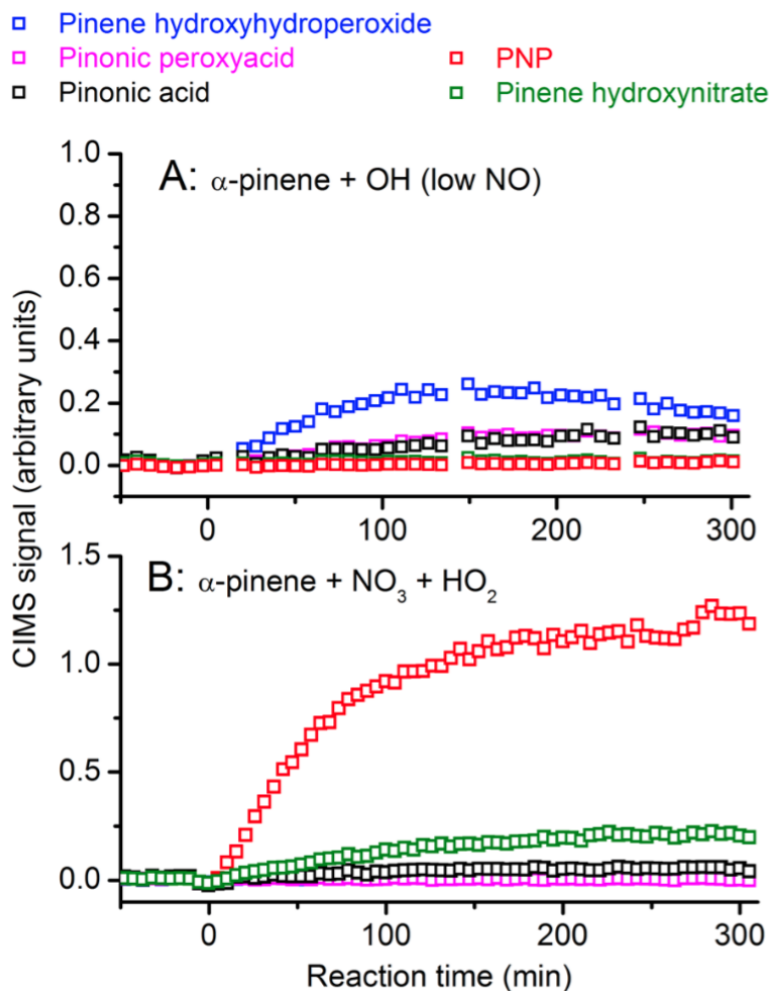


Figure C.13: Ion intensity data (not converted to mixing ratio) from the negative ion mode CIMS during control experiments performed with α -pinene: (A) The pinene nitrooxyhydroperoxide (PNP, red markers) used as a tracer for NO₃ in this work is not formed under the low-NO conditions that were used to photooxidize MPAN; (B) PNP is only formed (and is a major product) when NO₃ is available to oxidize α -pinene (or β -pinene) in the presence of HO₂ radicals (generated from photolysis of HCHO in these experiments). Pinonaldehyde (measured in positive ion mode, not shown) is also a major product in both oxidation experiments.

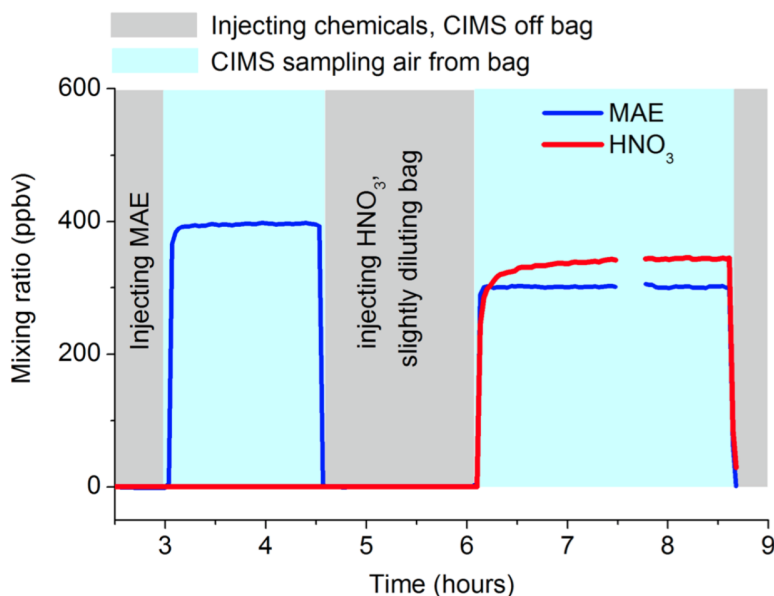


Figure C.14: Monitoring the loss of MAE to the walls of a 1000 L Teflon bag, filled with dry purified ("zero") air (relative humidity < 5% in the bag). MAE did not demonstrate any observable wall loss under these conditions. Injections of nitric acid (~500 ppbv injected, ~300 ppbv observed in the gas phase) did not change the wall loss behavior of MAE over the course of 2.5 hours, after which the instrument was taken off the bag.

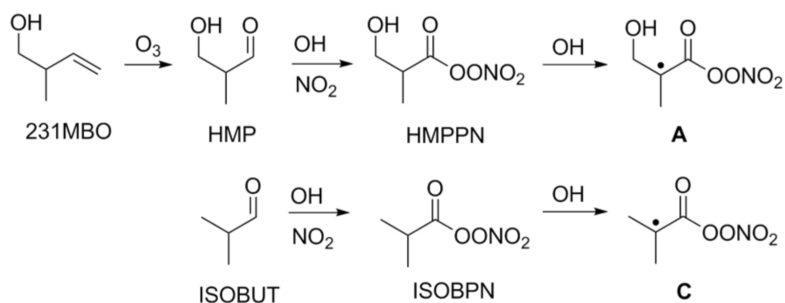


Figure C.15: Gas-phase synthesis of β -alkyl radicals from saturated APNs: hydroxymethylpropanoyl peroxyxynitrate (HMPPN) and isobutanoyl peroxyxynitrate (ISOBPN).

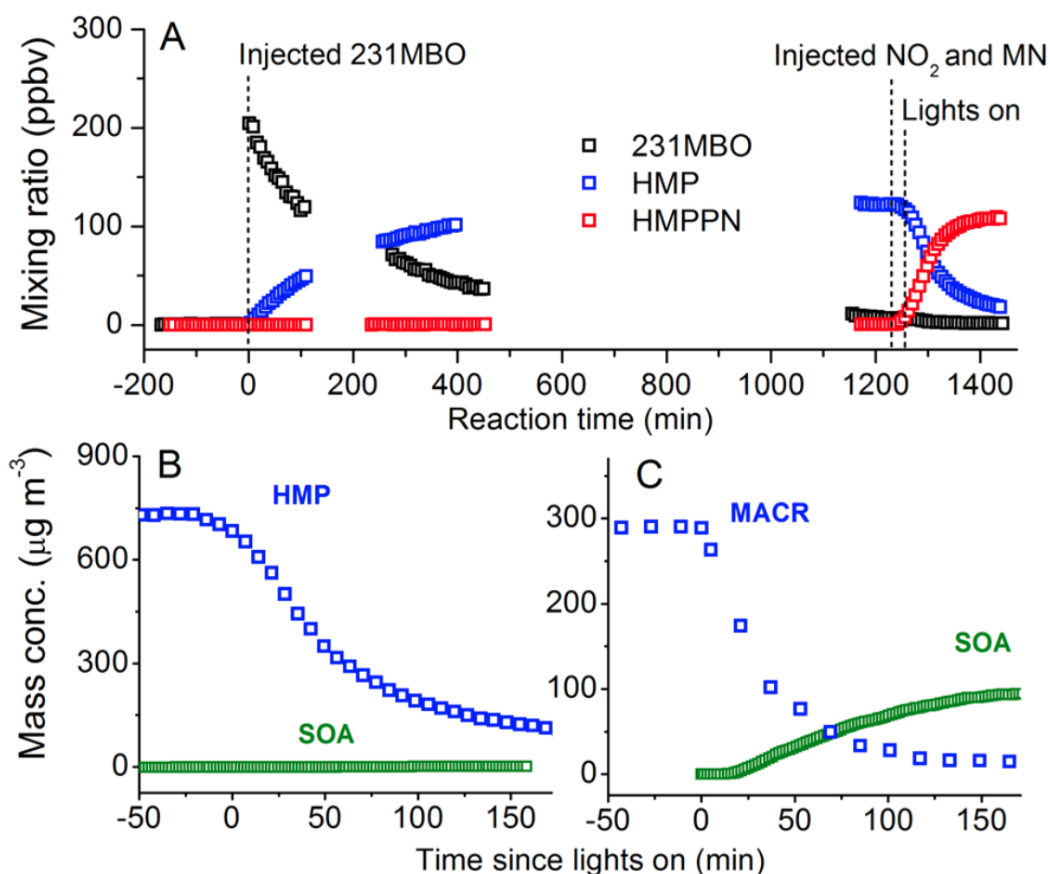


Figure C.16: SOA formation from saturated vs. unsaturated APNs: (A) the results from Expt. 11 where 231MBO is ozonized into its aldehyde HMP, followed by high-NO₂ photooxidation to the APN (HMPPN) with methyl nitrite (MN) as an OH precursor; (B) the reaction shown in panel A where the time axis is renormalized to start when UV lights are switched on and SOA from the dark period is subtracted; (C) similar to panel B but with MACR as the hydrocarbon (Expt. 9). Both vertical axes in panels B and C are with respect to mass. Breaks in data occur when instruments are not sampling from the chamber.

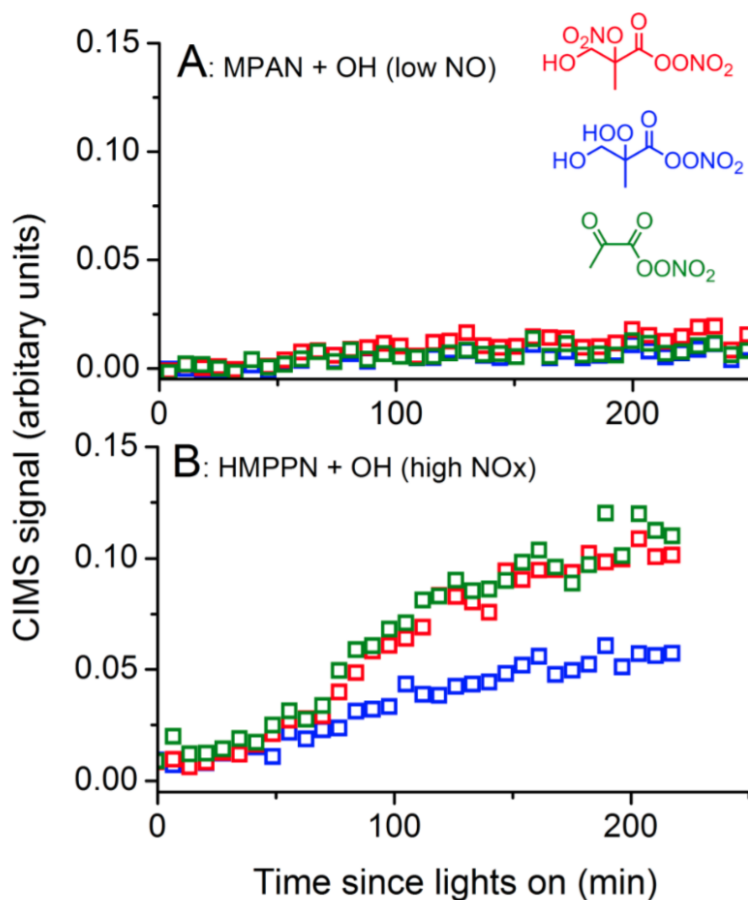


Figure C.17: High-NO and low-NO compounds from alkylperoxyl (RO_2) radical B: the hydroxynitrates ($\text{RO}_2 + \text{NO} \rightarrow \text{RONO}_2$, red), hydroxyhydroperoxides ($\text{RO}_2 + \text{HO}_2 \rightarrow \text{ROOH} + \text{O}_2$, blue), and 2-oxopropanoyl peroxyxynitrate (2OPN, green) from (A) the MPAN photooxidation and (B) the HMPPN photooxidation. The production of HAC from MPAN (reaching ~ 0.25 at the 250 min mark) and HMPPN (reaching 1.8 at the 220 min mark), *via* different mechanisms, is greater than the production of the shown compounds.